SRF 951220-18

# Cutoff Frequencies of Several SRF and CESR Beam Pipes.

S. Belomestnykh
Laboratory of Nuclear Studies, Cornell University, Ithaca, NY 14853

## 1 Introduction: Why did I write this note?

Having analyzed the interaction of a beam with the superconducting RF (SRF) cavity, I came to the necessity to learn what are cutoff frequencies of different beam pipe cross-sections. Superconducting cavity design [1] for the CESR luminosity upgrade plan is called BB1. It has two beam tubes of a big diameter to allow higher order modes (HOMs) to propagate toward the ferrite HOM dampers [2]. One of those tubes, round beam tube (RBT), has cutoff frequency just enough to be above resonant frequency of the fundamental mode, but below resonant frequency of the second monopole HOM. Unfortunately, the lowest dipole HOM does not propagate in the round beam tube. The other beam tube, fluted beam tube (FBT), has four special flutes which reduce the cutoff frequency of the dipole mode below the resonance of the lowest dipole HOM, but at the same time they do not greatly affect the cutoff of monopole modes. In a recent beam test the BB1-1 cavity [3] had adjacent CESR beam pipes of a different cross-sections. I call them FBT end beam pipe and RBT end beam pipe. In the final location of the superconducting cavities in CESR they will have regular CESR beam pipes on both ends. It is important to know the cutoff frequencies of the beam pipes because above those frequencies HOM power begins to propagate in the beam pipe and we have to take this effect into account.

That is why I calculated those frequencies using SuperLANS [4, 5]. As it was the first time I used the program for that kind of calculations, I ran it for the sample problem of a circular waveguide and compared results with analytic ones. Then I calculated several cases of interest: the fluted beam tube, beam pipes adjacent to the cavity during beam test, and regular CESR beam pipe. All calculations were done in early 1995 and were reported at the SRF meeting of March 15 [6]. Later we used the frequencies obtained to understand some results of the beam test as well as for prediction of some aspects of the beam-cavity interaction in the future.

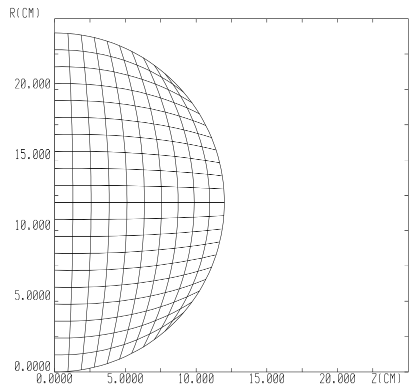


Figure 1: Circular Waveguide: Mesh

To my surprise, several people showed their interest in these calculations, especially to the cutoff frequencies of the CESR beam pipe. This interest and the wish to make the results more easily available forced me to write this paper.

## 2 Test Problem: Circular Waveguide

In so far as a choice of a test problem is orbitrary to some extent, I chose my “favorite” circular waveguide. Cutoff wavelength and frequency for the circular waveguide are [7]:

$$(\lambda)_{TMnl} = \frac{1}{\sqrt{\mu\epsilon}(f_c)_{TMnl}} = \frac{2\pi a}{p_{nl}};$$

$$f_{c,[MHz]} = \frac{4771.35 p_{nl}}{a_{[cm]}} \qquad (\mu = \mu_0, \epsilon = \epsilon_0);$$

$$(\lambda)_{TEnl} = \frac{1}{\sqrt{\mu\epsilon}(f_c)_{TEnl}} = \frac{2\pi a}{p'_{nl}};$$

$$f_{c,[MHz]} = \frac{4771.35 p'_{nl}}{a_{[cm]}} \qquad (\mu = \mu_0, \epsilon = \epsilon_0);$$

where $p_{nl}$ is the $l$-th root of $J_n(x) = 0$, $p_{nl} = (k_c)_{nl} a$, $p'_{nl}$ is the $l$-th root of $J'_n(x) = 0$, $p'_{nl} = (k_c)_{nl} a$, $a$ is the radius of the waveguide, $J_n$ and $J'_n$ are Bessel function of order $n$ and its derivative. One can find first several roots in Table 1 and Table 2 [8].

For the SuperLANS calculations I chose the radius of the circular waveguide equal to 12 cm which corresponds to the radius of the round beam tube of the BB1 cavity. The mesh of $10 \times 20$ elements was used (Figure 1). The results of calculations in comparison with analytic numbers are presented in Table 3. Also, field lines of the lowest two TM and TE modes are shown in Figures 2-5. We know from the URMEL calculations [9] that resonant frequency of the lowest dipole mode is equal to 641.505 MHz which is lower than cutoff frequency of the $TE_{11}$ mode of the RBT, i.e. that dipole mode is trapped inside the cavity and therefore can not be damped by ferrite HOM loads.

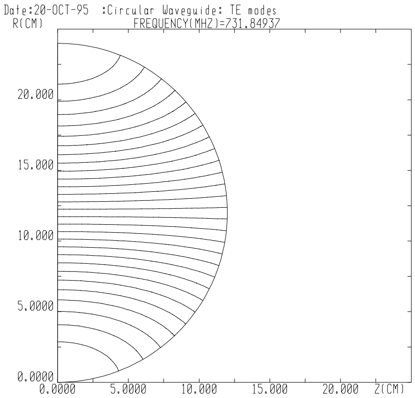


Figure 2: Circular Waveguide: $TE_{11}$

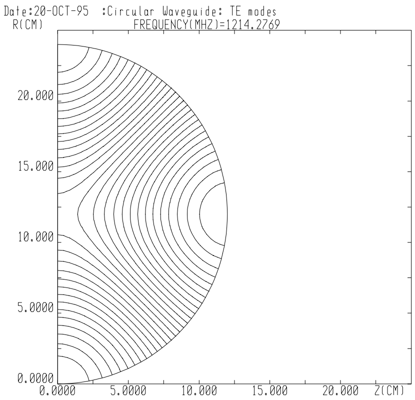


Figure 3: Circular Waveguide: $TE_{21}$

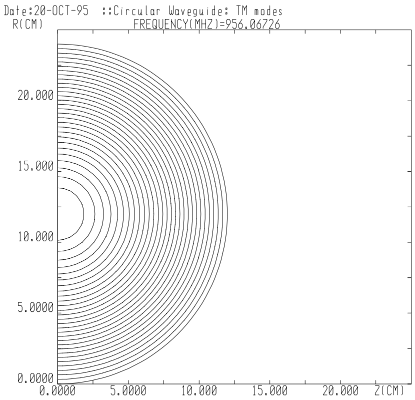


Figure 4: Circular Waveguide: $TM_{01}$

# 3 Results of Calculations

## 3.1 Fluted Beam Tube

A beam tube of a special, fluted, shape is used in the BB1 superconducting cavity to allow lowest dipole higher-order modes to propagate toward the HOM ferrite load. Systematic calculations of the cutoff frequency of the $TE_{11}$ mode were performed in wide range of possible flute sizes [1]. But somehow it happened that the cutoff frequency was not calculated for the case of the final design. That is why I calculated cutoffs for this case. The cross-section and the mesh are shown in Figure 6, results are presented in Table 4, and field lines for the two lowest $TM$ and $TE$ HOMs are shown in Figures 7-10. Effective radius, $a_{\text{eff}}$, is the radius of the circular waveguide which has the same cutoff frequency of given mode. Now we see that cutoff frequency of the $TE_{11}$ mode is much lower with flutes. In the same time the resonant frequency of the lowest cavity dipole mode is affected just a little bit by flutes: it was measured 607 MHz for the copper full size model of the cavity with tapers [9, 10]. So, all dipole modes can propagate toward the HOM load and thus be damped.

## 3.2 FBT End Beam Pipe

FBT end beam pipe cross-section and used mesh are shown in Figure 11. This shape looks more elliptical. Unfortunately, I could not figure out simple way to do analytical calculations of cutoff frequencies for elliptical waveguide. Nevertheless, I compared cutoffs for these two cases using SuperLANS' results for both of them.

Table 1: Zeros of Bessel Functions, $J_n(x)$.

| $l$ | $n=0$ | $n=1$ | $n=2$ | $n=3$ | $n=4$ |
|---|---|---|---|---|---|
| 1 | 2.40483 | 3.83171 | 5.13562 | 6.38016 | 7.58834 |
| 2 | 5.52008 | 7.01559 | 8.41724 | 9.76102 | 11.06471 |
| 3 | 8.65373 | 10.17347 | 11.61984 | 13.01520 | 14.37254 |
| 4 | 11.79153 | 13.32369 | 14.79595 | 16.222347 | 17.61597 |

Table 2: Zeros of Derivatives of Bessel Functions, $J_n'(x)$.

| $l$ | $n=0$ | $n=1$ | $n=2$ | $n=3$ | $n=4$ |
|---|---|---|---|---|---|
| 1 | 3.83171 | 1.84118 | 3.05424 | 4.20119 | 5.31755 |
| 2 | 7.01559 | 5.33144 | 6.70613 | 8.01524 | 9.28240 |
| 3 | 10.17347 | 8.53632 | 9.96947 | 11.34592 | 12.68191 |
| 4 | 13.32369 | 11.70600 | 13.17037 | 14.58585 | 15.96411 |

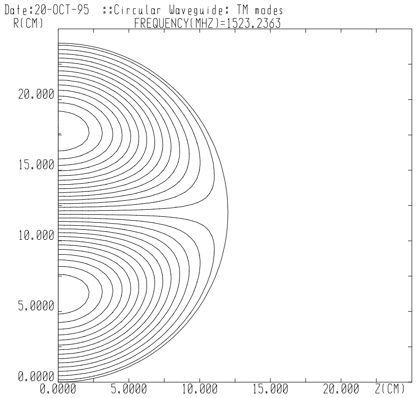


Figure 5: Circular Waveguide: $TM_{11}$

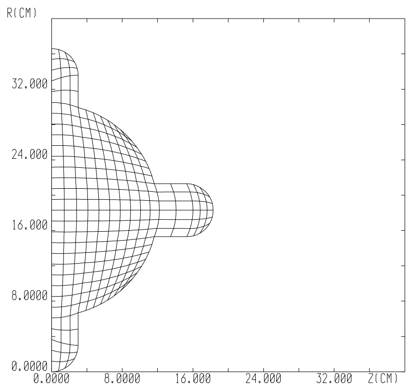


Figure 6: Fluted Beam Tube: Mesh

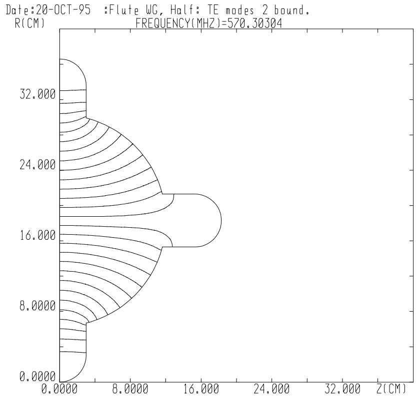


Figure 7: Fluted Beam Tube: $TE_{11}$

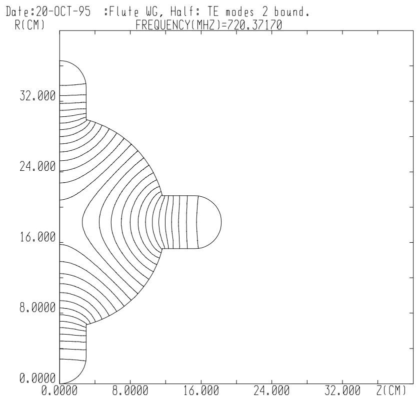


Figure 8: Fluted Beam Tube: $TE_{21}$

Table 3: Cicular Waveguide: Comparison of SuperLANS and Analytic Calculations.

| mode type | $f_{SLANS}, MHz$ | $f_{analytic}, MHz$ | $\frac{f_{SLANS}-f_{analytic}}{f_{analytic}}$ |
|---|---|---|---|
| $TE_{11}$ | 731.849 | 732.076 | $-3.1 \cdot 10^{-4}$ |
| $TE_{21}$ | 1214.277 | 1214.404 | $-1.0 \cdot 10^{-4}$ |
| $TE_{01}$ | 1523.351 | 1523.532 | $-1.2 \cdot 10^{-4}$ |
| $TE_{31}$ | 1670.291 | 1670.446 | $-9.3 \cdot 10^{-5}$ |
| $TE_{41}$ | 2114.042 | 2114.324 | $-1.3 \cdot 10^{-4}$ |
| $TE_{12}$ | 2119.476 | 2119.847 | $-1.8 \cdot 10^{-4}$ |
| $TE_{51}$ | 2550.618 | 2550.931 | $-1.2 \cdot 10^{-4}$ |
| $TE_{22}$ | 2666.334 | 2666.441 | $-4.0 \cdot 10^{-5}$ |
| $TE_{02}$ | 2789.366 | 2789.482 | $-4.2 \cdot 10^{-5}$ |
| $TM_{01}$ | 956.067 | 956.186 | $-1.2 \cdot 10^{-4}$ |
| $TM_{11}$ | 1523.236 | 1523.536 | $-2.0 \cdot 10^{-4}$ |
| $TM_{21}$ | 2041.794 | 2041.987 | $-9.5 \cdot 10^{-5}$ |
| $TM_{02}$ | 2194.674 | 2194.849 | $-8.0 \cdot 10^{-5}$ |
| $TM_{31}$ | 2536.667 | 2536.832 | $-6.5 \cdot 10^{-5}$ |
| $TM_{12}$ | 2789.175 | 2789.486 | $-1.1 \cdot 10^{-4}$ |
| $TM_{41}$ | 3017.155 | 3017.219 | $-2.1 \cdot 10^{-5}$ |
| $TM_{22}$ | 3347.242 | 2041.987 | $1.3 \cdot 10^{-4}$ |
| $TM_{03}$ | 3441.113 | 3440.827 | $8.3 \cdot 10^{-5}$ |
| $TM_{51}$ | 3487.864 | 3487.650 | $6.1 \cdot 10^{-5}$ |

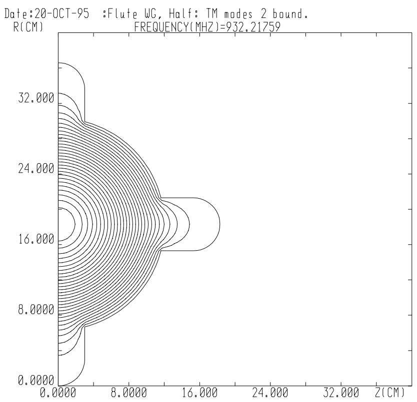


Figure 9: Fluted Beam Tube: $TM_{01}$

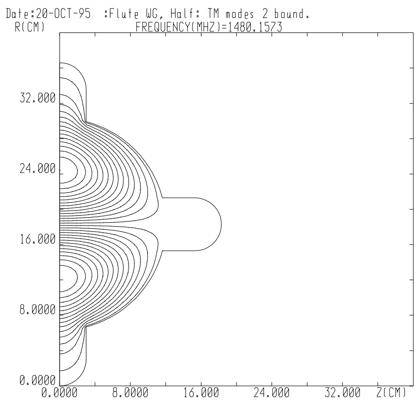


Figure 10: Fluted Beam Tube: $TM_{11}$

Table 4: Fluted Beam Tube.

| mode type | $f_{SLANS}, MHz$ | $a_{eff.}, cm$ |
|---|---|---|
| $TE_{11}$ | 570.265 | 15.405 |
| $TE_{21}$ | 720.372 | 20.230 |
| $TE_{01}$ | 985.119 | 18.559 |
| $TE_{31}$ | 1136.814 | 17.633 |
| $TE_{02}$ | 1617.571 | 20.694 |
| $TE_{22}$ | 1633.896 | 19.583 |
| $TE_{32}$ | 1837.277 | 20.815 |
| $TE_{12}$ | 2173.437 | 11.704 |
| $TE_{41}$ | 2258.932 | 11.232 |
| $TM_{01}$ | 932.217 | 12.309 |
| $TM_{11}$ | 1480.157 | 12.352 |
| $TM_{21}$ | 1916.070 | 12.789 |
| $TM_{02}$ | 2108.725 | 12.490 |
| $TM_{31}$ | 2399.960 | 12.684 |
| $TM_{12}$ | 2687.871 | 12.454 |
| $TM_{41}$ | 2719.280 | 13.315 |
| $TM_{22}$ | 2865.231 | 14.017 |
| $TM_{51}$ | 3081.139 | 13.832 |
| $TM_{03}$ | 3195.895 | 12.920 |

Parameters of the used ellipse are:

$$A = 12.98448\ cm, \quad B = 9.37768\ cm,$$

$$e = 0.692, \quad q = 4.490\ cm, \quad s = 32.398\ cm,$$

where $A$ is the major axis, $B$ is the minor axis, $e$ is the eccentricity, $2q$ is the focal spacing, $s$ is the circumference. Circular waveguide classification of the HOMs is used in Table 5 because classification of the HOMs is a little bit complicated for the elliptical case. One can see that the elliptical shape provides quite a good approximation. Effective radius of the circular waveguide for the $TM_{01}$ mode is 5.254 cm. One can use this radius as a radius of the beam pipe in $2D$ calculations. Figures 12-13 show lowest $TE$ and $TM$ modes.

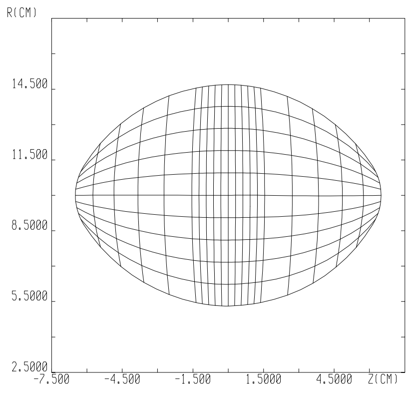


Figure 11: Fluted End Beam Pipe: Mesh

Table 5: FBT End Beam Pipe.

| mode type | $f_{FBTendbeampipe}, MHz$ | $f_{ell.}, MHz$ |
|---|---|---|
| $TE_{11}$ | 1410.411 | 1367.518 |
| $TE_{11}$ | 1874.947 | 1843.940 |
| $TE_{21}$ | 2460.140 | 2447.385 |
| $TE_{21}$ | 2820.745 | 2687.249 |
| $TE_{31}$ | 3484.308 | 3469.866 |
| $TM_{01}$ | 2184.000 | 2131.854 |
| $TM_{11}$ | 3216.701 | 3115.279 |
| $TM_{11}$ | 3718.495 | 3652.183 |
| $TM_{21}$ | 4697.122 | 4541.288 |
| $TM_{21}$ | 4258.186 | 4144.900 |

Table 6: RBT End Beam Pipe.

| mode type | $f_{SLANS}, MHz$ | $f_{rect.}, MHz$ |
|---|---|---|
| $TE_{10}$ | 1120.893 | 1111.753 |
| $TE_{20}$ | 2241.250 | 2220.251 |
| $TE_{01}$ | 3284.341 | 3256.858 |
| $TE_{30}$ | 3360.541 | 3330.377 |
| $TE_{11}$ | 3500.978 | 3440.857 |
| $TM_{11}$ | 3442.106 | 3440.857 |
| $TM_{21}$ | 3943.937 | 3941.654 |
| $TM_{31}$ | 4661.888 | 4661.660 |
| $TM_{41}$ | 5512.540 | 5506.831 |

## 3.3 RBT End Beam Pipe

RBT end beam pipe had an almost rectangular cross section (Figure 14). That is why cutoffs of this beam pipe are compared with cutoffs of a rectangular waveguide of 13.503 cm × 4.603 cm in Table 6. One can see that a rectangular waveguide is a good approximation for this case. Effective radius of the circular waveguide for the $TM_{11}$ mode is 3.333 cm. Figures 15-16 present field lines of the lowest $TE$ and $TM$ modes.

## 3.4 CESR "Elliptical" Beam Pipe

This case is of special interest because results could be very helpful in understending beam interaction with various discontinuities in the CESR vacuum chamber, sliding joint for example [11]. The cross-section of the regular CESR vacuum chamber is very close to elliptical (Figure 17). The results are compared for these two cross-sections in Table 7. Ellipse parameters are:

$$A = 9\ cm, \quad B = 5\ cm,$$

$$e = 0.831, \quad q = 3.752\ cm, \quad s = 20.840\ cm.$$

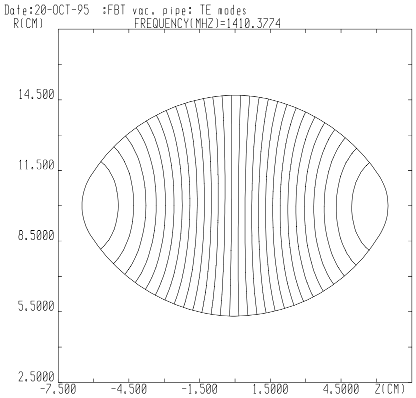


Figure 12: Fluted End Beam Pipe: $TE$ mode

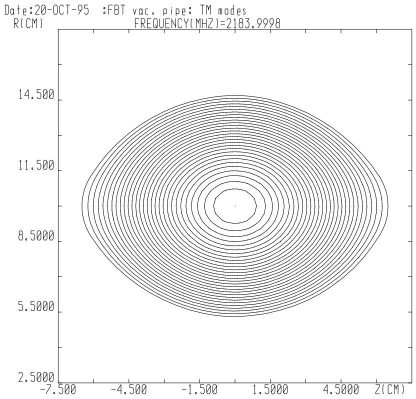


Figure 13: Fluted End Beam Pipe: $TM$ mode

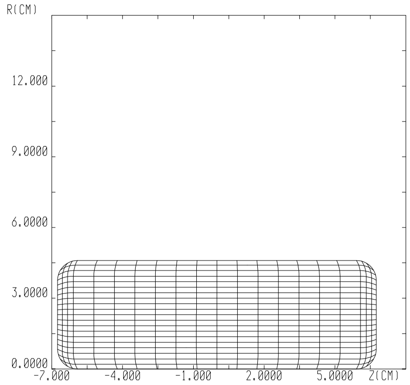


Figure 14: Round End Beam Pipe: Mesh

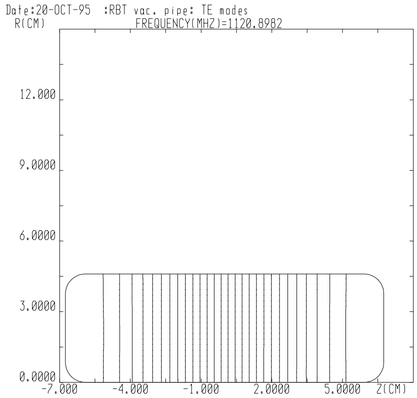


Figure 15: Round End Beam Pipe: $TE_{10}$

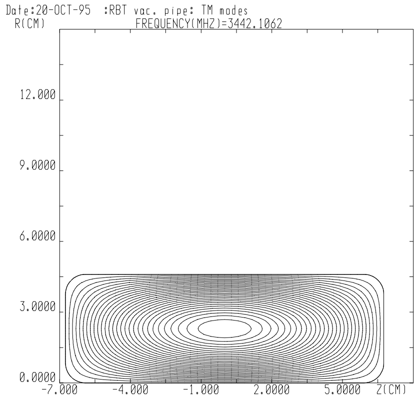


Figure 16: Round End Beam Pipe: $TM_{11}$

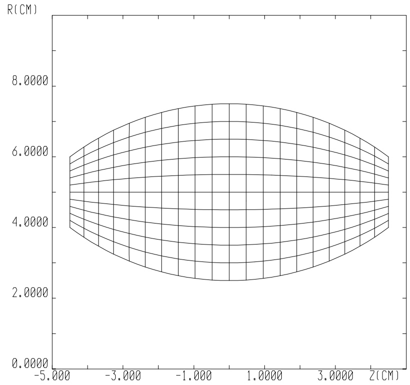


Figure 17: CESR Beam Pipe: Mesh

Table 7: CESR Beam Pipe.

| mode type | $f_{CESR}, MHz$ | $f_{ell.}, MHz$ |
|---|---|---|
| $TE_{11}$ | 1914.745 | 1983.580 |
| $TE_{11}$ | 3407.333 | 3399.520 |
| $TE_{21}$ | 3475.199 | 3607.156 |
| $TE_{21}$ | 4556.398 | 4581.693 |
| $TE_{31}$ | 5044.870 | 5186.255 |
| $TM_{01}$ | 3683.648 | 3695.385 |
| $TM_{11}$ | 4975.796 | 5033.595 |
| $TM_{21}$ | 6340.699 | 6464.401 |
| $TM_{11}$ | 6618.967 | 6612.238 |
| $TM_{21}$ | 7770.938 | 7833.912 |

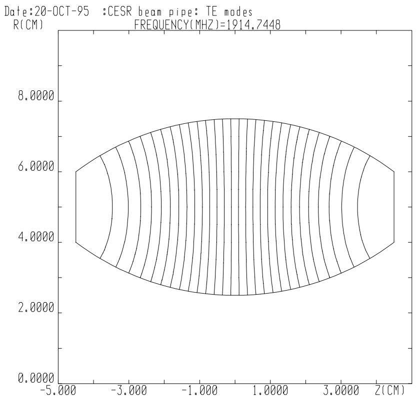


Figure 18: CESR Beam Pipe: $TE$ mode

Effective radius of the circular waveguide for the $TM_{01}$ mode is 3.115 cm. Two lowest $TE$ and $TM$ modes are shown in Figures 18-21.

# 4 Conclusion

The cutoff frequencies of beam pipes of several cross-sections were calculated using SuperLANS. The results of calculations were already used in analysis of the beam-SRF cavity interaction as well as beam-sliding joint interaction and, I hope, will be useful in the future.

# References

[1] *H. Padamsee, et al.* Design Challenges for High Current Storage Rings, *Particle Accelerators,* Vol. 40, pp. 17-41 (1992).

[2] *S. Belomestnykh, et al.* Comparison of the Predicted and Measured Loss Factor of the Superconducting Cavity Assembly for the CESR Upgrade, *presented at the 1995 Particle Accelerator Conference,* Dallas,

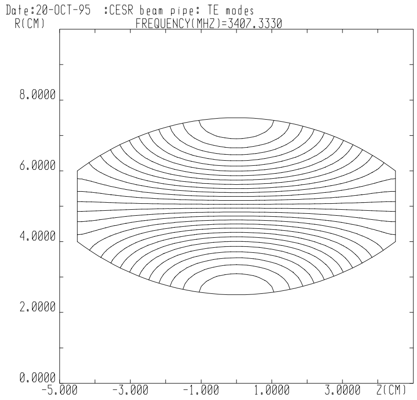


Figure 19: CESR Beam Pipe: $TE$ mode

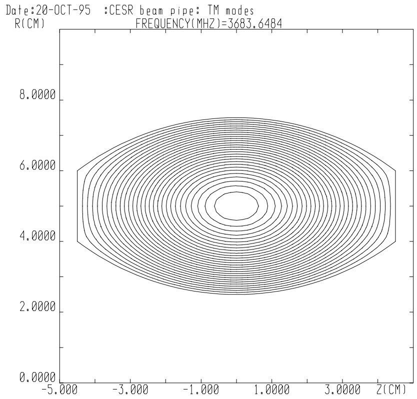


Figure 20: CESR Beam Pipe: $TM$ mode

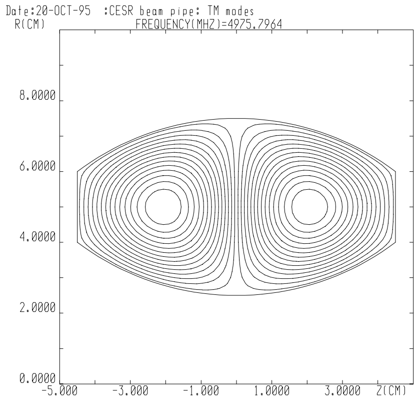


Figure 21: CESR Beam Pipe: $TM$ mode

TX, May 1995, also *Report SRF 950406-04,* Cornell Laboratory of Nuclear Studies, Ithaca, NY (April 1995).

[3] *H. Padamsee et al.* Beam Test of a Superconducting Cavity for the CESR Luminosity Upgrade, *presented at the 1995 Particle Accelerator Conference,* Dallas, TX, May 1995, also *Report SRF 950501-08,* Cornell Laboratory of Nuclear Studies, Ithaca, NY (May 1995).

[4] *D. Myakishev, et al.* SUPERLANS/SUPERSAM Codes. User's Guide, Novosibirsk, Russia, 1992, also *Report SRF/D 940314-02,* Cornell Laboratory of Nuclear Studies, Ithaca, NY (March 1994).

[5] *D. G. Myakishev, V. P. Yakovlev.* An Interactive Code SUPERLANS for Evaluating of RF Cavities and Acceleration Structures, *Conf. Record of the 1991 IEEE Particle Accelerator Conference,* San Francisco, CA, May 1991, Vol. 5, pp. 3002-3004.

[6] Minutes of the SRF Meeting, March 15, 1995, *Report SRFM 031595,* Cornell Laboratory of Nuclear Studies, Ithaca, NY (March 1995).

[7] *S. Ramo, J. R. Winnery, T. van Duzer.* Fields and Waves in Communication Electronics, *John Wiley & Sons,* NY, 1967.

[8] *Ed. by M. Abramowitz and I. Stegun.* Handbook of Mathematical Functions with Formulas, Graphs, and Mathematical Tables, *Dover Publications,* NY, 1972.

[9] Minutes of the SRF Meeting, July 9, 1992, *Report SRFM 070992,* Cornell Laboratory of Nuclear Studies, Ithaca, NY (July 1992).

[10] *V. Veshcherevich, et al.* Higher Order Modes Damping in CESR-B Cavity, *Proceedings of "B Factories: The State of the Art in Accelerators, Detectors and Physics", SLAC-4000/CONF-9204126,* Stanford, CA, April 1992, pp. 177-180.

[11] *Z. Greenwald, S. Greenwald.* CESR's Sliding Joints Study: Loss Parameter, Trapped Modes and Bunch Train Wakes, *Report CON 95-05,* Cornell Laboratory of Nuclear Studies, Ithaca, NY (June 23, 1995).